GFD 2017 Lecture 9: Greenland Glacier-Ocean Interaction Part I

Fiamma Straneo; notes by Margaret Lindeman, Agostino Meroni, and Earle Wilson

June 29, 2017

1 The Near Ice Zone

1.1 Diagnosing the influence of subglacial discharge

The Greenland Ice Sheet (GIS) is losing mass at an accelerated rate and is responsible for approximately 25% of the current rate of global sea-level rise (Church et al., 2011; Chen et al., 2017). Much of this mass loss occurs via the release of ice and melt water at outlet glaciers, which terminate in deep and narrow fjords (van den Broeke et al., 2009). Here it is argued that the mass loss is in part affected by the release of subglacial melt water into the ocean.

Subglacial discharge is due to large catchments upstream of the glacier's marine interface and has a peak discharge of approximately 30×10^3 m^3/s during summer months (Jackson and Straneo, 2016). This seasonal discharge of subglacial meltwater can be diagnosed from glacier-induced changes in water properties in Sermilik Fjord, the fjord adjacent to Helheim Glacier. Figure 1 shows distributions of potential temperature and salinity in the Sermilik Fjord for the summer of 2009 (left) and the winter of 2010 (right).

Ambient waters within the fjord can be modified by two glacial sources of freshwater: subglacial discharge and submarine melt. Subglacial discharge is assumed to be fresh and at its local freezing point at depth. If no other sources of freshwater are present, mixing between the deep ambient waters of the fjord and the cold, fresh subglacial discharge water from beneath glacier results in a modified water mass whose properties lie along the *runoff line* indicated by the dashed line in Figure 1. Submarine melt modifies the ambient water in a similar fashion but causes additional ocean cooling through the extraction of latent heat. If no other sources of freshwater are present, the melting of the ice and its subsequent mixing with ambient ocean water will result in a new water mass that lies along the *melting line* indicated by the solid line in Figure 1.

Figure 1 shows that, during the summer months, the waters of the Sermilik Fjord are modified by both runoff/subglacial discharge and submarine melt. The is evidenced by the fact that the near-glacier fjord water has a $\theta - S$ distribution that lies between the runoff

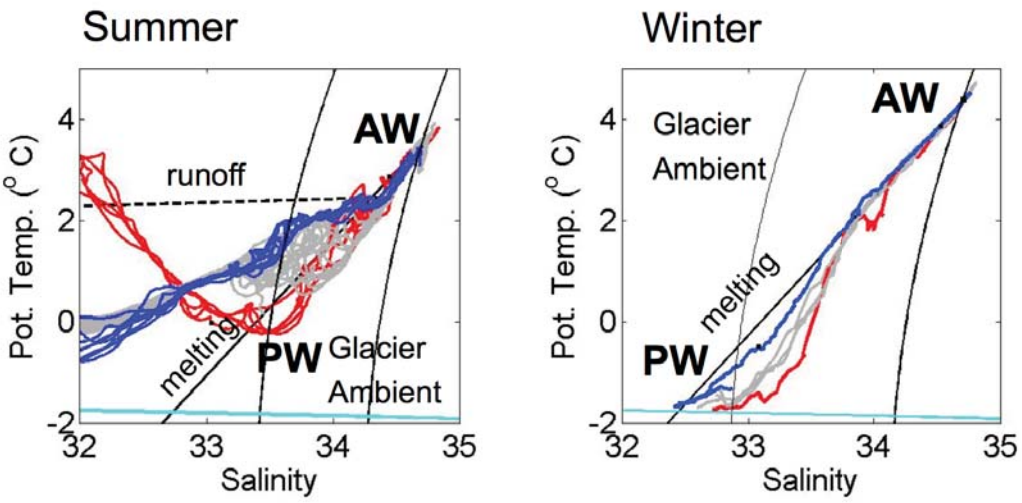

Figure 1: Seasonal distribution of water mass properties in the Sermilik Fjord. Left: Potential temperature (θ) versus salinity (S) of the ocean at the mouth of the fjord (red) and near the glacier (blue) collected in August 2009. Right: Same, but for March 2010. The dashed and solid line represent the mixing lines for runoff and submarine melt, respectively. The cyan line shows the freezing point of seawater for different salinities. Figure is adapted from Straneo et al. (2011).

and melt lines. During the winter months, the $\theta - S$ distribution of the ocean indicates that submarine melt is the main source of freshwater for the fjord.

If the ambient waters consist of a single water mass, the relative contributions of freshwater from submarine melt and subglacial discharge can be quantified (e.g Mortensen et al., 2011; Jackson and Straneo, 2016).

1.2 Dynamics at the ice-ocean interface

When subglacial discharge enters the ocean at the grounding line, it rises as a turbulent buoyant plume. The mixing generated by this turbulent plume enhances the exchange of heat between the ambient ocean and the ice surface, thereby elevating the submarine melt rate. Since submarine melting has a primary control on the mass balance of the entire ice sheet, it is essential that we understand the dynamics of this interaction.

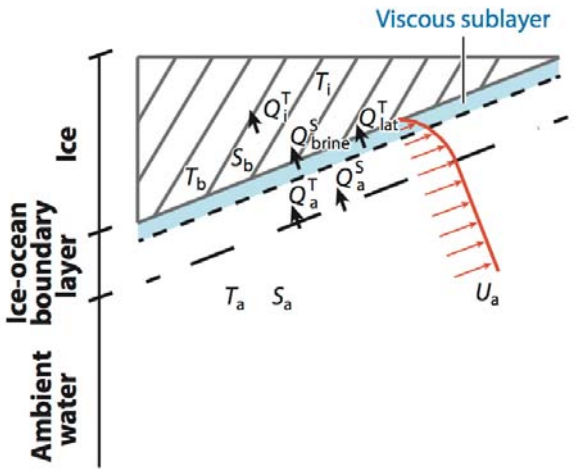

Figure 2: A schematic describing the processes governing the temperature, salinity and melt rate at the ice-ocean interface. Q_a^T is the heat flux from the ambient fjord water to the glacier, Q_i^T is the heat flux into the ice, and Q_{lat}^T is the latent heat flux from phase changes. Corresponding freshwater fluxes are denoted by the superscript S with the addition of Q_{brine}^S, associated with the melting or freezing of ice. All other variables are defined in the text. Figure is taken from Straneo and Cenedese (2015), which is modified from Holland and Jenkins (1999).

The submarine melt rate is typically determined through the use of a three-equation plume model. This model, which was first developed for the floating ice shelves of Antarctica, solves for the temperature T_b, salinity S_b and melt rate $\dot{m}$ at the ice-ocean interface(Hellmer and Olbers, 1989; Holland and Jenkins, 1999). A schematic of the processes represented by the model is provided in Figure 2.

T_b is constrained to be at the in situ freezing point of seawater, which is governed by

$$T_b = \lambda_1 S_b + \lambda_2 + \lambda_3 p_b, \tag{1}$$

where λ_1, λ_2 and λ_3 are known constants, and Z_b is the pressure at the interface. T_b and S_b are further constrained by the heat and salt fluxes across the viscous sublayer that separates the ice boundary from the ambient ocean. The heat budget of the viscous sublayer is a balance of the heat flux supplied by the ambient ocean and the sensible and latent heat flux to the ice

$$C_p \gamma_T (T_a - T_b) = \dot{m} C_i (T_b - T_i) + \dot{m} L, \tag{2}$$

where T_a is the ambient ocean temperature, C_p and C_i are the specific heat capacities of seawater and ice, L is the latent heat of fusion, and γ_T is the thermal exchange velocity. Likewise, the salt budget of the viscous sublayer is a balance of the salt flux supplied by the ambient ocean and the salt flux across the ice boundary. This is given by

$$\gamma_S (S_a - S_b) = \dot{m} (S_b - S_i), \tag{3}$$

where γ_S is the salinity exchange velocity, S_a is the salinity of the ambient ocean and S_i is the salinity of the ice, which is sometimes assumed to be zero. In the turbulent region outside the viscous sublayer, heat and salt diffuse at the same rate. However, within the viscous sublayer, the exchange of heat and salt are governed by molecular diffusion. In this region, heat is transferred at a faster rate than salt. Additionally, these exchange rates are dependent on the shear generated by the ambient ocean as it drags along the ice. These effects are parameterized as

$$\gamma_{T,S} = C_D^{\frac{1}{2}} \Gamma_{T,S} U_a, \tag{4}$$

where $C_D^{\frac{1}{2}} \Gamma_{T,S}$ represents the thermal and haline Stanton numbers for a hydraulically smooth surface (Kader and Yaglom, 1972; Steele et al., 1989).

From equations (1)-(4), we see that an increase in near-ice ocean velocity U_a, will lead to an increase in the submarine melt rate $\dot{m}$. This velocity can be influenced by either large scale ocean circulation, driven by processes like tidal motions, or by local buoyant plumes supplied by subglacial discharge. For the near-vertical calving fronts typically found in Greenland, the latter mechanism is dominant, especially during summer months (Sciascia et al., 2013).

A major caveat to the three-equation model is that it was developed for the near horizontal floating ice-shelves of Antarctica. The tidewater glaciers of Greenland have a much steeper ocean interface and receive much greater freshwater input from subglacial discharge. These differences likely affect the turbulent exchange rates parameterized by (4).

1.3 Plume modeling

The ultimate goal of plume modeling is to predict the submarine melt rate (SMR) along the front of a glacier. The SMR will depend on the plume's buoyancy forcing, vertical extent and lateral extent. Additionally, the vertical structure and velocity of the nearby ocean will also have an impact. Due to the paucity of in situ data, many of these factors remain largely unconstrained. We therefore rely on models to inform our understanding of these processes.

Plume models currently fall into two broad categories: simple one-dimensional buoyant plume models (e.g. Hellmer and Olbers, 1989; Jenkins, 2011) based on buoyant plume theory originally developed by Morton et al. (1956) and Turner (1973), and fully three-dimensional plume models that utilize physics from high-resolution, non-hydrostatic general circulation models (e.g. Sciascia et al., 2013; Slater et al., 2015). In each case, the subglacial discharge forcing the plume may be funneled through a single point source, a distribution of small point sources or across the full width of the grounding line.

One-dimensional plume models have been used to varying degrees of success to explain observations of water mass properties near tidewater glaciers. For example, Stevens et al. (2016) showed that the line plume model introduced by (Jenkins, 2011) is able to reproduce the measured vertical extent and composition of glacially modified waters near a major subglacial discharge site at the Saqqarliup sermia outlet glacier system in West Greenland. However, the same model was unable represent the properties of glacially modified waters at another nearby subglacial discharge site. This discrepancy was attributed to uncertainties

in subglacial discharge and missing physics (such as the detachment of the plume after it reaches neutral buoyancy).

Other studies have used three-dimensional plume models to quantify the sensitivity of SMR to certain unknown parameters. For example, Slater et al. (2015) showed that subglacial discharge, when distributed over a wide area, could produce up to five times as much submarine melt as when the amount of discharge is passed through a single localized outlet. Additionally, Sciascia et al. (2013) showed that the intrusion depth of a buoyant plume will depend on the magnitude of the subglacial discharge. These sensitivity studies highlight the great uncertainty surrounding SMR and stresses the need for more observational studies.

1.4 Summary

1. The seasonal injection of subglacial discharge affects ice-ocean exchanges by affecting the dynamics at the interface.

2. Plume models work well near the glacier front, but the far-field impacts of plumes is not represented by these models.

3. Melt rates from models are highly uncertain, to a large extent because they have not been validated by data.

2 Fjord Dynamics

Many tidewater glaciers, especially in Greenland, do not have terminate in open ocean waters, but in a fjord. The fjord connects the glacier and its catchment, which are influenced by the atmospheric dynamics of the region, with the open ocean circulation, which determines the heat input to the glacier front, all of which influence ice sheet and grounding line dynamics. Due to the inherent difficulties in performing field campaigns in these regions, the fjord dynamics is still a topic of very active research. The fjord circulation is known to be mainly driven by the freshwater input of the subglacial discharge (Motyka et al., 2003; Rignot et al., 2010), the along-fjord katabatic winds that flow downhill from the ice-sheet and the along-shelf winds that drive the so-called intermediary circulation, by imposing density fluctuations at the mouth of the fjord itself (Jackson et al., 2014). Additionally, processes of deep water renewal and transient motions (namely internal waves or internal seiches) characterize the fjord circulation.

2.1 Iceberg trajectories

Using GPS trackers such as the one in figure 3, icebergs can be tracked until they completely melt or capsize. The sensors are deployed from a helicopter, on large icebergs with a waterline length longer than 100 m. The motion of large icebergs is primarily driven by the ocean currents, rather than wind.

Figure 3: Picture of a GPS tracker placed on the surface of a large iceberg in the Sermilik Fjord (South-East Greenland) from a helicopter. (Photo by F. Straneo)

Observations of iceberg trajectories through GPS tracking show a net mean displacement of the ice mélange, a mixture of icebergs and sea ice extending $O(10$ km) beyond the glacier front, out of the fjord (Sutherland et al., 2014). In particular, multiple icebergs in the mélange are observed to undergo sudden simultaneous motions. These are caused either by strong calving events at the glacier front or by the action of intense katabatic winds that can flush the whole ice mélange out of the fjord in few days. Figure 4, from Sutherland et al. (2014), shows the daily average distance from the glacier front of three icebergs in the ice mélange as a function of time deployed. The average velocities marked on the intervals of constant slope shows that the mélange is a compact system that moves at a roughly constant speed for its whole extension. The sudden changes in position that happens in two or three days (around day 120) indicates a strong calving event that pushed the entire mélange out of the fjord. After this first phase of motion, the icebergs, if they do not capsize or become trapped by bottom topography, are observed to move on average out of the fjord until they reach the open ocean, where they are driven south-westward by the East Greenland Coastal Current. This mean displacement is indicative of the buoyancy-driven estuarine-like circulation due to the subglacial runoff at the glacier front (Motyka et al., 2003; Rignot et al., 2010).

2.2 Buoyancy-driven circulation

As mentioned earlier, the freshwater released at the base of the glacier front has been observed to form plumes that rise buoyantly near the glacier front, entraining ambient water until they reach the surface or a neutral buoyancy depth. This gives rise to a buoyancy-driven circulation, with the relatively cold, fresh plume detaching from the glacier front and flowing toward the fjord mouth, while the entrainment drives flow of warmer, saltier Atlantic Water

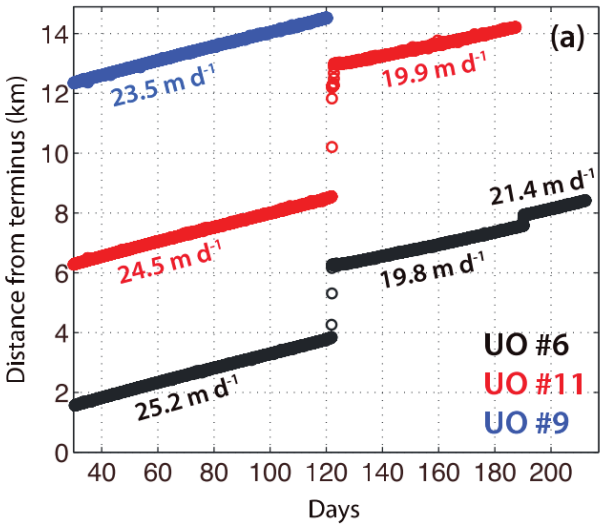

Figure 4: Displacement from the glacier terminus of three icebergs in the ice mélange in the Sermilik Fjord in South-East Greenland as a function of the time deployed (Sutherland et al., 2014).

toward the glacier (Straneo and Cenedese, 2015). Figure 5 shows a scheme of this kind of circulation, highlighting the salty water input on the bottom of the fjord and the relatively fresher water export at the surface (Rignot et al., 2010).

The flux of subglacial discharge and resulting entrainment of ambient water thus have a strong influence on the heat flux to the glacier front from warm Atlantic Water. Observations of enhanced submarine melting corresponding to the buoyant plumes have shown a strong seasonal variability, corresponding to the seasonality of subglacial discharge, which has a maximum in summer or after intense rainfalls (Motyka et al., 2003). Moreover, it was found that submarine melting can contribute to the ice-sheet mass balance as significantly as the calving, making it an important factor in grounding-line and ice-flow dynamics (Rignot et al., 2010).

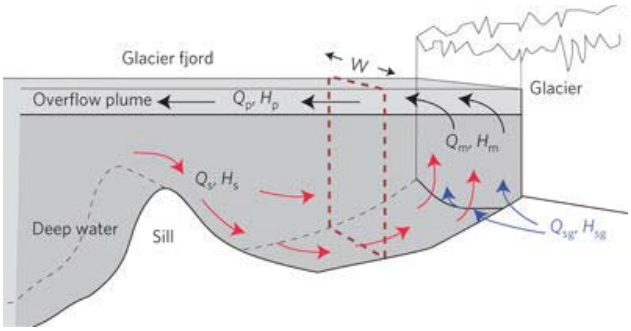

Figure 5: Scheme of the estuarine-like circulation observed in the fjords driven by the positively buoyant freshwater input of the subglacial runoff. In most fjords, the dynamics is almost two-dimensional and small across-fjord variations are generally observed (Rignot et al., 2010).

Exercise: *The importance of heat transport from outside a fjord can be shown with a simple calculation using typical characteristics of each fjord and glacier, as given in table 1. What would the change in mean fjord temperature be if the entire ice flux from each glacier was melted by water in the fjord?*
The necessary input of heat is calculated as the heat needed to warm the ice to its freezing point plus the heat needed for the phase change:

$$Q_H = \rho_i Q_i \left[c_i (T_\mathrm{f} - T_i) + L \right] * 1 \text{ year}. \tag{5}$$

The change in fjord temperature is calculated as

$$\Delta T = \frac{Q_H}{c_w \rho_w V_\mathrm{fjord}}, \tag{6}$$

where $V_\mathrm{fjord} \equiv l * w * d$. Inputting the values from table 1 gives a temperature decrease of approximately 8^oC for Sermilik Fjord and 1^oC for 79 North Fjord. With no renewal of water from outside the fjord, this would bring the temperature of both fjords below freezing. This exercise is indicative of the importance of heat transport from outside the fjords to maintain a steady state balance between the fjord and glacier.

2.3 Observing seasonal variability

Moored observations of current velocities are crucial to understanding fjord dynamics during the non-summer months, when the subglacial runoff forcing is weak, but icebergs pose a significant challenge to collecting long timeseries of observations. Figure 6 shows how iceberg impacts may affect a mooring (Jackson, 2016). Panel (A) shows how the pressure measurements at three different levels all collapse to the bottom value simultaneously, indicating that the impact with an iceberg has pushed the buoy below a critical depth at which the water pressure has compressed it, so that is it no longer able to float. Panel (B) shows the

	79 North Glacier + Fjord	Helheim Glacier + Sermilik Fjord
Ice flux Q_i (km^3 yr^{-1})	15	30
Grounding depth d (m)	600	600
Width w (km)	20	6
Length l (km)	80	80
Ice temperature T_i (^{o}C)	-10	-10
Upper 100m water temp. (^{o}C)	T_f	T_f
Lower 500m water temp. (^{o}C)	1	4
Constants: Heat capacity of ice c_i: 2 kJ kg^{-1} ^{o}C^{-1} Heat capacity of seawater c_w: 4 kJ kg^{-1} ^{o}C^{-1} Latent heat of fusion L: 334 kJ kg^{-1} Ice density ρ_i: $\sim$ 917 kg km^{-3} Seawater density ρ_w: $\sim$ 1025 kg km^{-3}		

Table 1: Estimates of typical characteristics of the 79 North Glacier and Fjord, Helheim Glacier, and Sermilik Fjord and pertinent physical constants to be used in the exercise.

track of the iceberg that hit the mooring and panel (C) contains a scheme for the two kinds of impact with an iceberg. In the type 1 hit, the buoy is not compressed and thus it still floats after the iceberg has passed, while in the type 2 hit, the buoy sinks after the pressure has squeezed it, as shown in the picture of panel (D).

Using timeseries of moored observations in Sermilik Fjord, a new decomposition of the mass, salt and heat budgets that include mechanisms that have been neglected in the past literature is introduced (Jackson and Straneo, 2016). Two major circulation regimes are identified: shelf variability via barrier winds (dominant in nonsummer months) and freshwater discharge from runoff (dominant in summer).

2.4 Other drivers of fjord circulation

Figure 7 shows the timeseries of along-fjord velocity (a,b) and potential temperature (c,d) at two different locations in the Sermilik fjord.(Jackson et al., 2014). The moorings that survived the season show that the currents have a strong variability on the $O(2-3$ days) scale, associated with the periodic tilting of the halocline at the mouth of the fjord due to the atmospheric mesoscale forcing. When cyclonic winds blow along the continental shelf in front of the south-eastern coasts of Greenland (see figure 8), the Ekman transport induces an increase in pressure in the upper layer at the mouth of the fjord. This generates an overturning circulation that opposes the buoyancy-driven one. This explains the short scales O(days) variability in the direction of the fjord circulation, as opposed to the monthly variations induced by the subglacial runoff forcing that controls the estuarine-like circulation

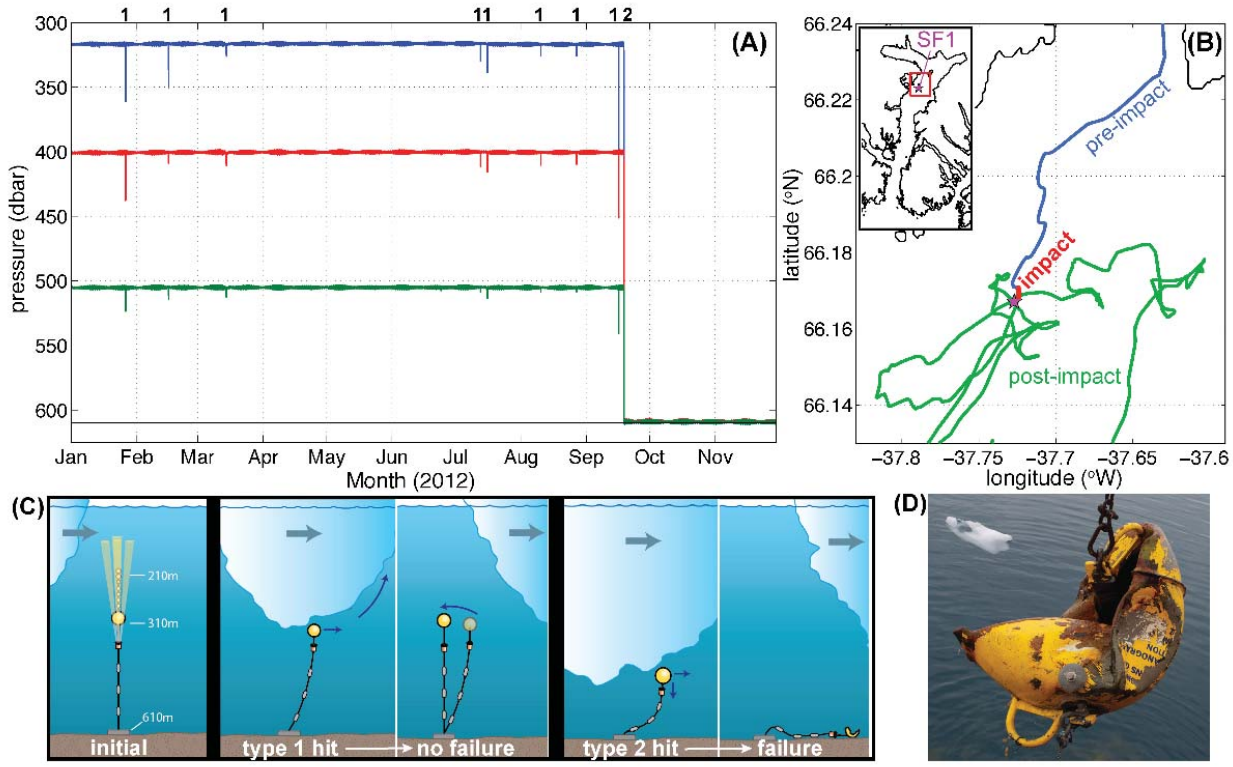

Figure 6: (A) pressure measurements before and after the impact with the iceberg. (B) Track of the iceberg. (C) Schemes of the two types of impact, in the former the buoy is still able to float because the pressure has not deformed it, while in the latter the buoy has been pushed at such a depth that the it cannot sustain the water pressure and it sinks. (D) Picture of a buoy recovered after a type 2 hit (Jackson, 2016).

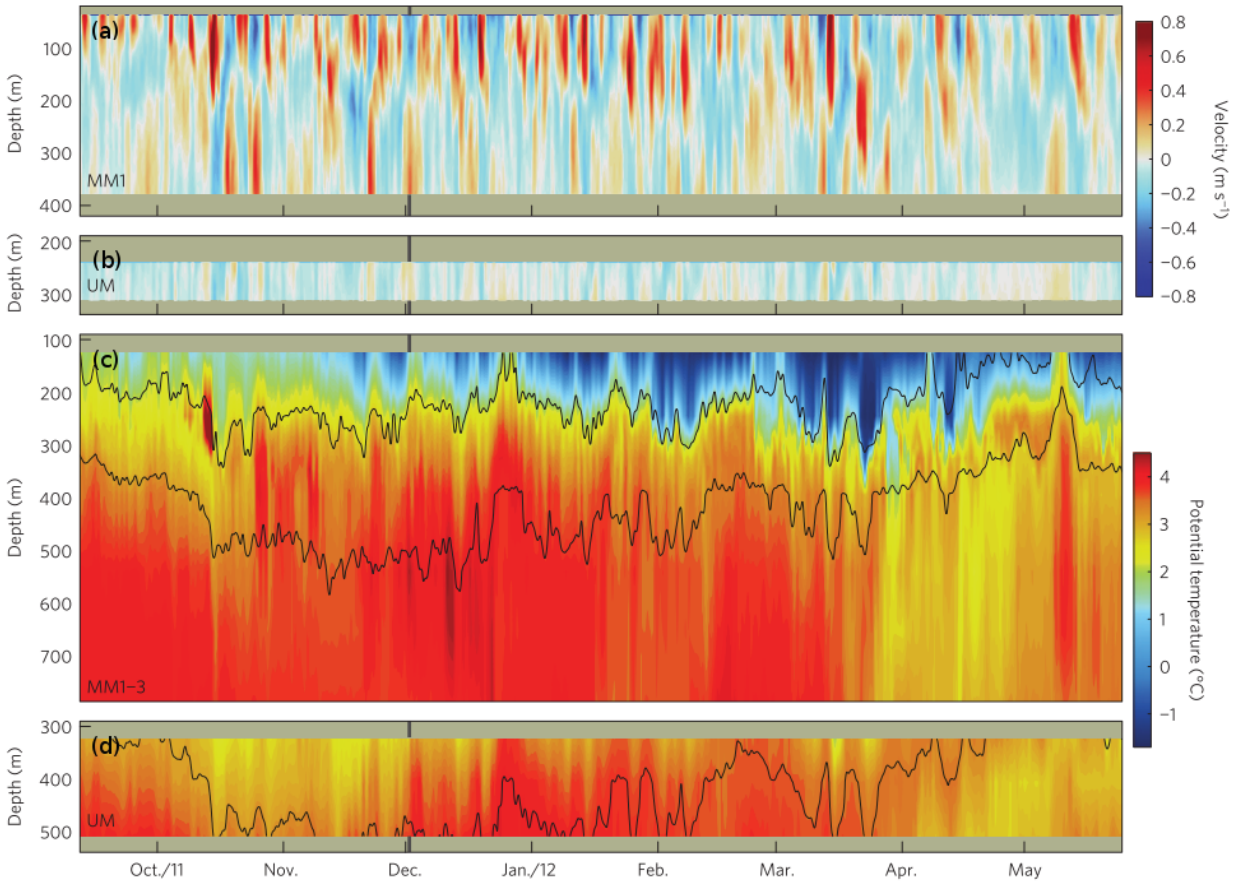

Figure 7: (a), (b) Along-fjord velocity (positive is towards the glacier) in two locations in the Sermilik fjord. (c), (d) Potential temperature timeseries for the same two locations with the contours of potential density anomaly $\sigma_\theta = [27.0, 27.5]$ kg m^{-3} overlaid. (b), (d) are closer to the glacier front than (a) and (c).'' Adapted from (Jackson et al., 2014).

described above.

The fjord circulation is also driven by along-fjord katabatic winds, which have been observed to flush out the entire ice mélange of a fjord on a O(1 day) scale. These winds, which blow from the ice sheet to the open ocean and can reach hurricane velocities, have a significant influence on the fjord circulation in the same direction as the buoyancy-driven one (Oltmanns et al., 2014, 2015). An example of this kind of event is shown in figure 9, where a series of three satellite images (Moderate Resolution Imaging Spectroradiometer, MODIS) shows how a strong wind event removes almost completely the ice mélange of the Ammassalik fjord in roughly one day (Oltmanns et al., 2014). Numerical simulations of a typical katabatic wind event in Greenland fjords show that $O(10\%)$ of the upper layer is flushed out in a single event, in agreement with observations (Spall et al., 2017).

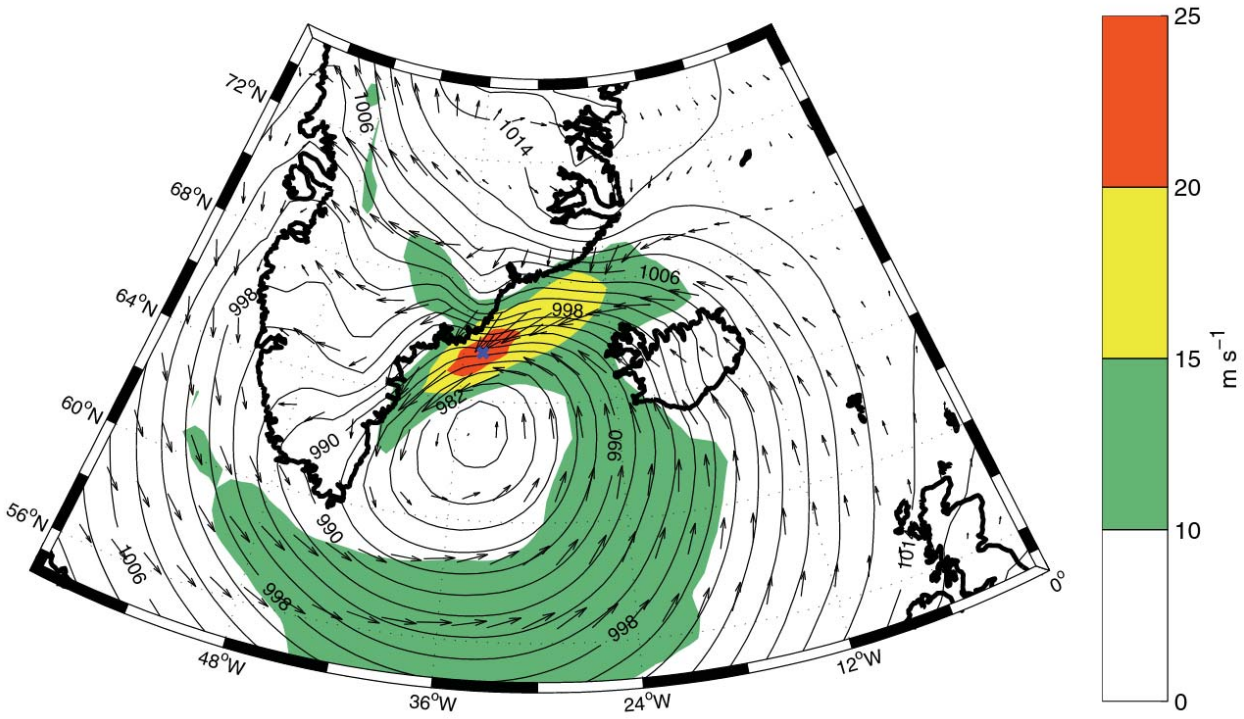

Figure 8: Composite analysis of the 10 meters winds (shading) and mean sea level pressure (contours) for the times of wind events over 15 m s^{-1} in the location indicated by the blue cross roughly between August 2009 and August 2013 (Harden et al., 2014).

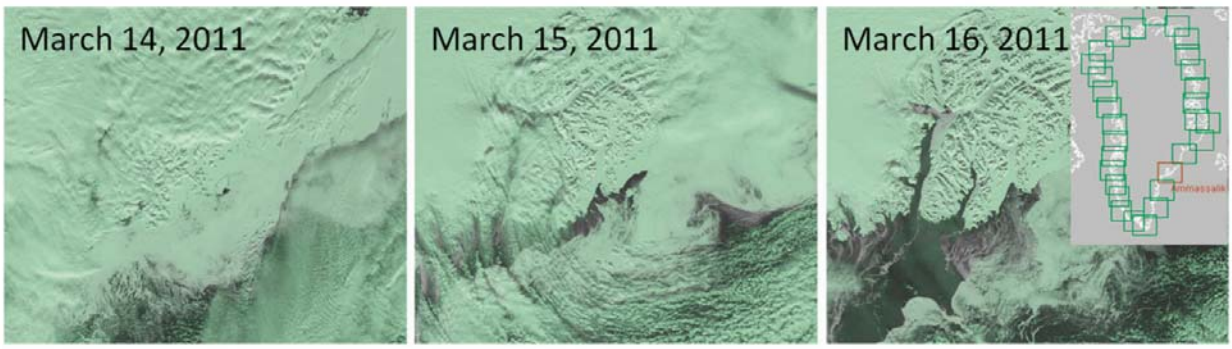

Figure 9: MODIS satellite images showing in the visible range the flushing of the ice mélange out of the Ammassalik fjord by the action of an intense katabatic wind event in roughly one day. Adapted from (Oltmanns et al., 2014).

2.5 Impact of topographic sills

With the same numerical setup it is possible to simulate the role of a sill in the fjord bottom topography, a feature present at the mouth of some glacial fjords. Numerical simulations by Gladish et al. (2015), focused on the water renewal in Illulisat Fjord, West Greenland, show that the position of the pycnocline with respect to the height of the sill is crucial in determining the circulation. In particular, a sill shallower than the pycnocline will block the inflow of warmer deep waters, reducing submarine melt at the glacier front. Moreover, numerical simulations show that while the subglacial runoff circulation can drive the water renewal in the fjord in a single summer, the external baroclinic forcing cannot, because of the presence of the sill blocking the flow at depth. The effect of a sill deeper than the pycnocline on the fjord water renewal mechanism is small.

2.6 Modeling the full fjord circulation

From the above discussion, it is evident that phenomena on multiple scales control the complex interaction between the ice-sheet and ocean components that characterize the Greenland coastal system. Examples of recent numerical efforts in modeling this broad range of processes, encompassing buoyant plumes due to the subglacial runoff at the glacier front, fjord buoyancy and wind circulation, iceberg displacement and open ocean dynamics include Carroll et al. (2015) and Cowton et al. (2015). The sensitivity of the glacier melting to the subsurface runoff, through the oceanic warmer water entrainment in the buoyant plume, is studied by means of numerical simulations by modifying the runoff flux and geometrical configuration (line plume versus point source plume, for example). Despite the lack of knowledge of some feedback mechanisms, for example between submarine melting and iceberg calving at the front, numerical results show that the submarine melt rates increase with subglacial runoff, but they appear to be insensitive to the annual runoff variability (Cowton et al., 2015). Instead, there is both numerical (Carroll et al., 2015) and observational (Beaird et al., 2015) evidence that the stratification at the glacier front influences the terminal level of a buoyant plume. In fact, depending on the depth profile of density, the subglacial runoff, and the turbulent entrainment, the plume can reach a neutral buoyancy level before surfacing. Other works are trying to model case studies of fjord circulation and to link the fjord variability to the large scale ocean variability.

2.7 Summary

1. Drivers of the circulation in the fjord include buoyancy due to meltwater release, regional winds, shelf-forced exchanges, tides.

2. The geometry of the fjord (sills, width, ice tongue extent) affects the circulation.

3. Theories of the fjord circulation typically do not cover the parameter space of the glacial fjords.

4. Future studies will need to explore the coupling between near-ice dynamics and fjord scale circulation, which are characterized by different length scales.

References

Beaird, N., Straneo, F., and Jenkins, W. (2015). Spreading of greenland meltwaters in the ocean revealed by noble gases. *Geophysical Research Letters*, 42(18):7705–7713. 2015GL065003.

Carroll, D., Sutherland, D. A., Shroyer, E. L., Nash, J. D., Catania, G. A., and Stearns, L. A. (2015). Modeling Turbulent Subglacial Meltwater Plumes: Implications for Fjord-Scale Buoyancy-Driven Circulation. *Journal of Physical Oceanography*, 45(8):2169–2185.

Chen, X., Zhang, X., Church, J. A., Watson, C. S., King, M. A., Monselesan, D., Legresy, B., and Harig, C. (2017). The increasing rate of global mean sea-level rise during 1993–2014. *Nature Climate Change*, 7(7):492–495.

Church, J. A., White, N. J., Konikow, L. F., Domingues, C. M., Cogley, J. G., Rignot, E., Gregory, J. M., van den Broeke, M. R., Monaghan, A. J., and Velicogna, I. (2011). Revisiting the Earth's sea-level and energy budgets from 1961 to 2008. *Geophysical Research Letters*, 38(18):n/a–n/a.

Cowton, T., Slater, D., Sole, A., Goldberg, D., and Nienow, P. (2015). Modeling the impact of glacial runoff on fjord circulation and submarine melt rate using a new subgrid-scale parameterization for glacial plumes. *Journal of Geophysical Research: Oceans*, 120(2):796–812.

Gladish, C. V., Holland, D. M., Rosing-Asvid, A., Behrens, J. W., and Boje, J. (2015). Oceanic Boundary Conditions for Jakobshavn Glacier. Part I: Variability and Renewal of Ilulissat Icefjord Waters, 2001–14*. *Journal of Physical Oceanography*, 45(1):3–32.

Harden, B. E., Straneo, F., and Sutherland, D. A. (2014). Moored observations of synoptic and seasonal variability in the East Greenland Coastal Current. *Journal of Geophysical Research: Oceans*, 119(12):8838–8857.

Hellmer, H. and Olbers, D. (1989). A two-dimensional model for the thermohaline circulation under an ice shelf. *Antarctic Science*, 1(04).

Holland, D. M. and Jenkins, A. (1999). Modeling Thermodynamic Ice–Ocean Interactions at the Base of an Ice Shelf. *Journal of Physical Oceanography*, 29(8):1787–1800.

Jackson, R. H. (2016). A mooring in iceberg alley. *Oceanus*, 51(2):16–19.

Jackson, R. H. and Straneo, F. (2016). Heat, Salt, and Freshwater Budgets for a Glacial Fjord in Greenland. *Journal of Physical Oceanography*, 46(9):2735–2768.

Jackson, R. H., Straneo, F., and Sutherland, D. A. (2014). Externally forced fluctuations in ocean temperature at Greenland glaciers in non-summer months. *Nature Geoscience*.

Jenkins, A. (2011). Convection-Driven Melting near the Grounding Lines of Ice Shelves and Tidewater Glaciers. *Journal of Physical Oceanography*, 41(12):2279–2294.

Kader, B. and Yaglom, A. (1972). Heat and mass transfer laws for fully turbulent wall flows. *International Journal of Heat and Mass Transfer*, 15(12):2329–2351.

Mortensen, J., Lennert, K., Bendtsen, J., and Rysgaard, S. (2011). Heat sources for glacial melt in a sub-Arctic fjord (Godthåbsfjord) in contact with the Greenland Ice Sheet. *Journal of Geophysical Research*, 116(C1):C01013.

Morton, B. R., Taylor, G., and Turner, J. S. (1956). Turbulent Gravitational Convection from Maintained and Instantaneous Sources. *Proceedings of the Royal Society A: Mathematical, Physical and Engineering Sciences*, 234(1196):1–23.

Motyka, R. J., Hunter, L., Echelmeyer, K. A., and Connor, C. (2003). Submarine melting at the terminus of a temperate tidewater glacier, LeConte Glacier, Alaska, U.S.A. *Annals of Glaciology*, 36:57–65.

Oltmanns, M., Straneo, F., Moore, G. W. K., and Mernild, S. H. (2014). Strong Downslope Wind Events in Ammassalik, Southeast Greenland. *Journal of Climate*, 27(3):977–993.

Oltmanns, M., Straneo, F., Seo, H., and Moore, G. W. K. (2015). The Role of Wave Dynamics and Small-Scale Topography for Downslope Wind Events in Southeast Greenland. *Journal of the Atmospheric Sciences*, 72(7):2786–2805.

Rignot, E., Koppes, M., and Velicogna, I. (2010). Rapid submarine melting of the calving faces of West Greenland glaciers. *Nature Geoscience*, 3(3):187–191.

Sciascia, R., Straneo, F., Cenedese, C., and Heimbach, P. (2013). Seasonal variability of submarine melt rate and circulation in an East Greenland fjord. *Journal of Geophysical Research: Oceans*, 118(5):2492–2506.

Slater, D. A., Nienow, P. W., Cowton, T. R., Goldberg, D. N., and Sole, A. J. (2015). Effect of near-terminus subglacial hydrology on tidewater glacier submarine melt rates. *Geophysical Research Letters*, 42(8):2861–2868.

Spall, M. A., Jackson, R. H., and Straneo, F. (2017). Katabatic Wind-Driven Exchange in Fjords. *Journal of Geophysical Research: Oceans*.

Steele, M., Mellor, G. L., and Mcphee, M. G. (1989). Role of the Molecular Sublayer in the Melting or Freezing of Sea Ice. *Journal of Physical Oceanography*, 19(1):139–147.

Stevens, L. A., Straneo, F., Das, S. B., Plueddemann, A. J., Kukulya, A. L., and Morlighem, M. (2016). Linking glacially modified waters to catchment-scale subglacial discharge using autonomous underwater vehicle observations. *The Cryosphere*, 10(1):417–432.

Straneo, F. and Cenedese, C. (2015). The dynamics of Greenland's glacial fjords and their role in climate. *Annu. Rev. Mar. Sci.*, 7:89–112.

Straneo, F., Curry, R. G., Sutherland, D. A., Hamilton, G. S., Cenedese, C., Våge, K., and Stearns, L. A. (2011). Impact of fjord dynamics and glacial runoff on the circulation near helheim glacier. *Nature Geoscience*, 4:322 EP –. Article.

Sutherland, D. A., Roth, G. E., Hamilton, G. S., Mernild, S. H., Stearns, L. A., and Straneo, F. (2014). Quantifying flow regimes in a Greenland glacial fjord using iceberg drifters. *Geophysical Research Letters*, 41(23):8411–8420.

Turner, J. S. (1973). *Buoyancy Effects in Fluids*. Cambridge University Press, Cambridge.

van den Broeke, M., Bamber, J., Ettema, J., Rignot, E., Schrama, E., van de Berg, W. J., van Meijgaard, E., Velicogna, I., and Wouters, B. (2009). Partitioning Recent Greenland Mass Loss. *Science*, 326(5955):984–986.